Rotated Quadrilateral Dipole UWB Antenna for Wireless Communication

Rajveer S. Brar[*], **Sarthak Singhal, and Amit K. Singh**

Abstract—A double printed rotated quadrilateral dipole UWB antenna for wireless communication is presented. The rotation of quadrilateral and modification of integrated balun structure is employed to enhance bandwidth and impedance matching. The proposed antenna shows impedance bandwidth of 3.8–18.1 GHz which covers the entire C, X and Ku bands. The radiation patterns of the designed antenna structure are relatively stable and omnidirectional over the entire obtained bandwidth with an average gain of 3.6 dB. A good agreement is found between the simulated and experimental results. The proposed antenna has a simple design, comparatively compact size and more bandwidth than previous reported double rhombus antenna.

1. INTRODUCTION

Ultra wideband (UWB) technology has become the most promising candidate for future short range and high speed wireless communication with less power dissipation. In 2002, Federal Communication Commission allocated frequency spectrum from 3.1–10.6 GHz for UWB applications [1]. UWB technology has the advantages of high data rate, low power dissipation, no interference to other standards, etc. Several antenna design techniques such as monopole, dipole, fractal, etc. are suitable for applications in UWB systems. Dipole antennas attract attention from researchers due to their easy impedance matching for UWB operation. Bow-tie dipole and diamond dipole are most basic dipole antennas presented for UWB operation [2]. Further, diamond shape is modified with rounded feeding edge and bow tie modified with rounded edge for bandwidth enhancement [3, 4]. Later rhombus antenna with array configuration is presented for phased array applications [5]. Bevelling of bow tie and circular cutout at the tip of a dipole are also used to enhance impedance bandwidth of dipole [6, 7]. Other dipole structures, such as rectangular, elliptical, and trapezoidal dipoles, are reported for UWB applications [8–10]. The circular wafer dipole antenna has enhanced bandwidth to cover partially Ku-band along with full coverage of C- and X-bands [11]. Some nonconventional optimized geometries have also been proposed in literature [12].

The demand for high data rate communication needs frequency to be shifted towards higher side. So application of Ku-band has received considerable attention during last decade, and a single antenna covering X band, C band and Ku Band is an exciting research topic. Matching balun is needed in dipoles to make it usable with 50 Ω systems [13]. But balun structures have narrowband impedance transition properties. So the design of balun having broadband impedance matching from unbalanced coaxial line to balanced dipole emerges as a major challenge for dipole antenna researchers. A balun transformer connects an unbalanced coaxial line to a balanced dipole structure, which prevents the distortion of antenna pattern and system performance variations by avoiding spurious currents on the sheath of the coaxial feed line [14].

* Corresponding author: Rajveer S. Brar (rajveer.singh.ece13@itbhu.ac.in).

The authors are with the Department of Electronics Engineering, Indian Institute of Technology (Banaras Hindu University), Varanasi-221005, India.

In this paper, the bandwidth of a quadrilateral dipole antenna is enhanced by rotating the dipole geometry and modifying ground balun structure. The antenna is designed and analysed by using Finite Element Method based Ansoft's High Frequency Structure Simulator software ver. 11 [15]. To analyse dispersion characteristics of the proposed antenna in impulse systems, time domain analysis is carried out by using Finite Integration Technique based CST Microwave Studio software [16]. Measurement of the fabricated prototype is performed to validate the simulation results.

2. ANTENNA DESIGN

The geometry of the designed antenna structure is shown in Fig. 1. The parameters are listed in Table 1. The proposed antenna is printed on a low cost FR-4 epoxy substrate of thickness 1.6 mm and $\varepsilon_r = 4.4$. The dielectric sheet is square of side length 31 mm. The designed antenna structure comprises a linearly tapered microstrip feed line, rotated quadrilateral dipole elements, and a modified ground balun structure loaded with symmetrical slits. Linearly tapered feed line is utilized for smooth transitions between the feed line and dipole elements.
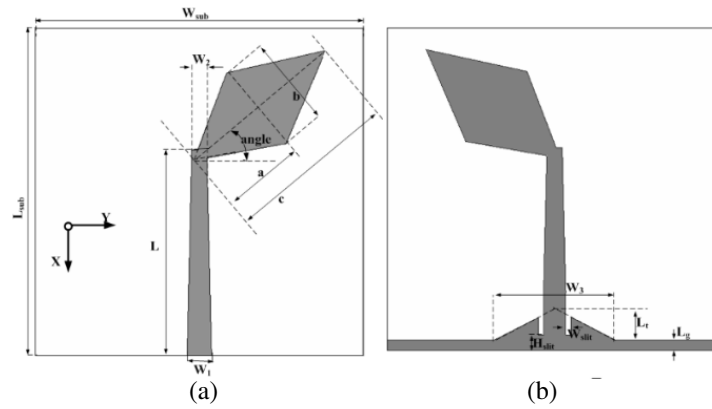

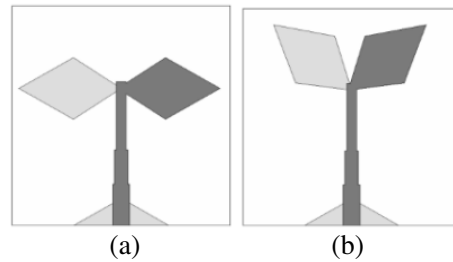**Figure 1.** Geometry of proposed antenna, (a) top layer, (b) bottom layer.

Figure 2. Quadrilateral dipole, (a) not rotated, (b) rotated.

Initially, a stepped microstrip line fed quadrilateral dipole antenna with triangular ground as shown in Fig. 2(a) is designed. To improve the impedance matching, rotation of quadrilateral structure is performed as shown in Fig. 2(b). Keeping the dipole patch shape rotated at optimised angle of 40°, the stepped structure is replaced by a linearly tapered structure as shown in Fig. 3. Linearly tapered feed has better impedance matching properties than stepped feed line due to reduction in the discontinuities at the step positions.

To improve balanced to unbalanced impedance transition, the triangular balun at ground plane is modified by joining a small rectangular structure near the base of balun. Now the overall ground balun structure is loaded with symmetrical slits near the taper feed line to shift upper cutoff frequency toward higher end as shown in Fig. 4. The truncated ground plane plays an important role in the broadband

Table 1. Antenna parameters.

Parameters	value (mm)	Parameters	value (mm)
L_{sub}	31	L	19.5
W_{sub}	31	w_3	11.2
a	7.7	L_t	3
b	8.8	L_g	1
c	16.2	Angle	$40°$
w_1	2.3	W_{slit}	0.5
w_2	1.4	H_{slit}	1.5

(a)   (b)
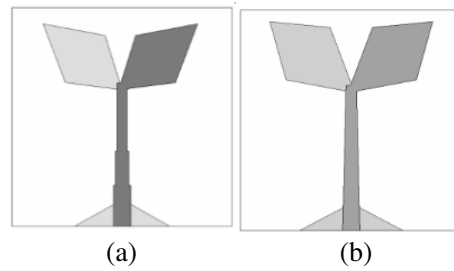
Figure 3. Feedlines (a) stepped, (b) linearly tapered.

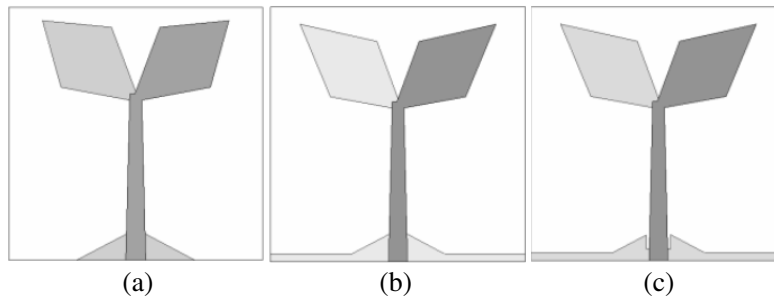(a)   (b)   (c)

Figure 4. Different ground balun structures, (a) triangle shape, (b) modified triangle with rectangle shape, (c) slits loaded modified balun shape.

characteristics of this antenna because it helps match the patch with the feed line in a wide range of frequencies. This is because the truncation creates a capacitive load that neutralizes the inductive nature of the patch to produce nearly pure resistive input impedance. The rectangular slits are used to control the impedance bandwidth and return loss level by modifying the capacitance between the patch and the ground plane.

3. RESULTS AND DISCUSSION

The reflection coefficient versus frequency characteristics of stepped fed quadrilateral dipole antenna for different angles of rotation is shown in Fig. 5. The geometry of quadrilateral dipole rotated at $0°$ and $40°$ is shown in Fig. 2. From Fig. 5, it is observed that with increase in the rotation angle from $0°$ to $40°$ the impedance matching is improved in the frequency band of 4–13.4 GHz. The resonance frequencies also shift towards lower frequency. At the rotation angle of $40°$, a new resonance at 15.4 GHz is also excited. It is observed that rotation improves impedance matching, keeping lower cutoff frequency constant and shifting the higher cutoff frequency of upper band slightly. Rotation principle converts a multi-band
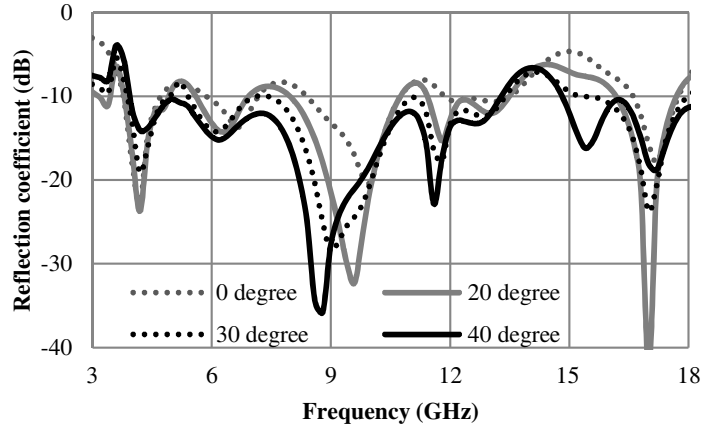
Figure 5. Comparison of reflection coefficient characteristics for quadrilateral and rotated quadrilateral.
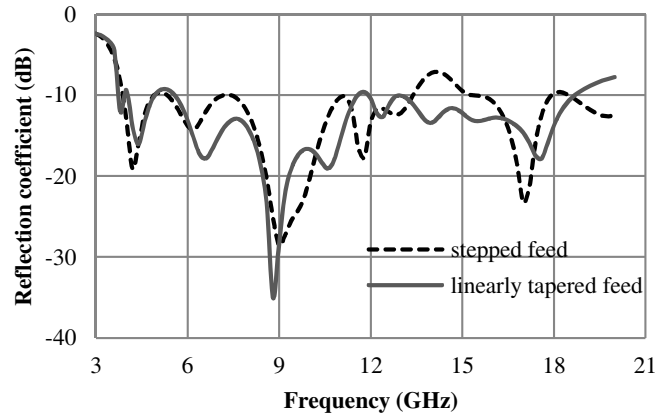

Figure 6. Comparison of reflection coefficient characteristics for stepped feed and linearly tapered feed.

antenna to dual-band antenna with lower band from 3.8 to 13 GHz and upper band from 15 to 18.1 GHz.

The reflection coefficient versus frequency characteristics for stepped microstrip line feed and linearly tapered feed is shown in Fig. 6. The dipoles with stepped microstrip feed and linearly tapered feed lines are shown in Figs. 3(a) and (b), respectively, while keeping rotated quadrilateral structure and triangular shape ground unchanged. It is observed that the impedance matching is improved at mid-frequencies, replacing the stepped feed line with a linearly tapered feed line. Tapered feed reduces the lower cutoff frequency slightly. This improvement in impedance matching occurs due to the smooth transitions between the radiating elements and feed line.

The reflection coefficient characteristics for different ground balun structures are shown in Fig. 7 and listed in Table 2. The geometry of all ground balun structures is shown in Fig. 4. It is observed that when a triangle balun structure is modified to rectangle added triangle ground balun structure, impedance matching at lower frequencies is improved by keeping lower cutoff frequency constant. But, there is no significant improvement in impedance matching at higher frequencies. Further loading of two symmetrical slits on modified balun shape enhances impedance matching at higher frequencies, keeping upper cutoff frequency to 18.1 GHz. The truncated ground plane plays an important role in the broadband characteristics of this antenna because it helps in matching the patch with the feed line in a wide range of frequencies. This is because the truncation creates a capacitive load that neutralizes the inductive nature of the patch to produce nearly pure resistive input impedance. The rectangular slits are used to control the impedance bandwidth and return loss level by modifying the capacitance between the patch and the ground plane.

The simulated and measured results of reflection coefficient of the proposed antenna are shown
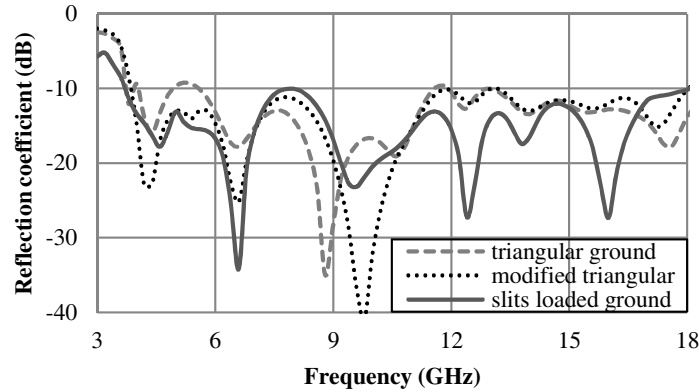
Figure 7. Comparison of reflection coefficient characteristics for different ground shapes.

Table 2. Comparison of different ground shapes.

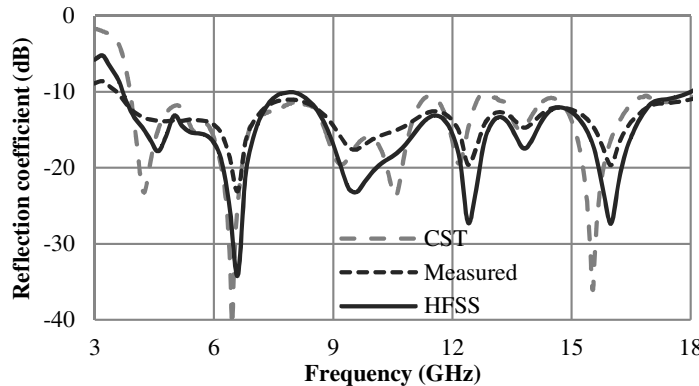| S. No.	Frequency (GHz)	Reflection Coefficient (dB)		
		Triangular ground	Modified triangular ground	Slit loaded ground
1	4.2	−14.7	−23	−14.7
2	5	−8	−13	−13
3	6.6	−18	−25.3	−34.2
4	9.8	−16.7	−40.8	−21.8
5	12.4	−11.7	−11.8	−27.2
6	16	−12.5	−12	−27.3

Figure 8. Variation of reflection coefficient with frequency.

in Fig. 8. The fabricated prototype is shown in Fig. 9. The experimental measurement of S_{11} for the designed prototype is carried out by using Anritsu's MS2038C VNA. The comparison between simulated and experimental results is also listed in Table 3. Simulation studies on two different analytical technique based simulators improve the reliability of simulation. It is observed that there is a good agreement between the experimental and simulated results, and a little difference is attributed to errors in soldering of SMA connecter to antenna structure.

The variation of real and imaginary parts of antenna input impedance with respect to frequency is shown in Fig. 10. It is observed that the real part is nearly equal to $50\,\Omega$ while the imaginary one is approximately $0\,\Omega$ for operating range. This leads to an observation that the designed antenna has

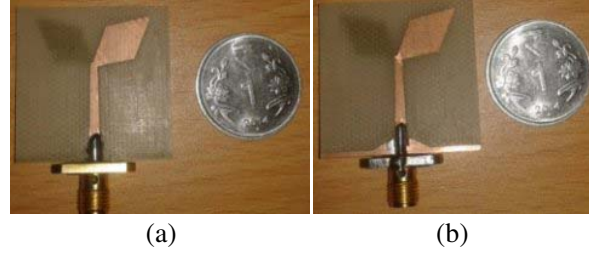(a)   (b)

Figure 9. The fabricated prototype, (a) top view, (b) bottom view.

Table 3. Comparison of HFSS, CST and measured results.

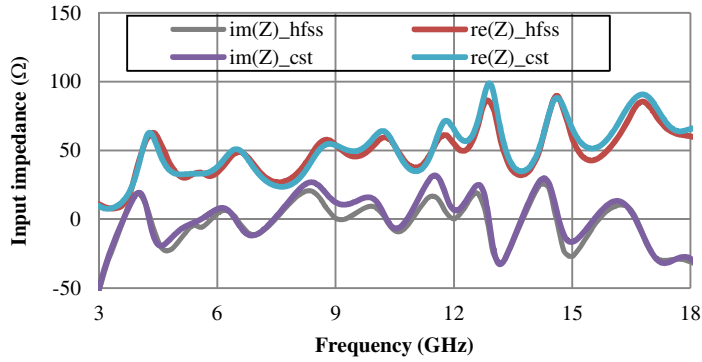| Software	f_L (GHz)	f_H (GHz)	BW (GHz)
HFSS	3.8	18.1	14.3
CST	3.9	18.1	14.2
Measured	3.8	18	14.1

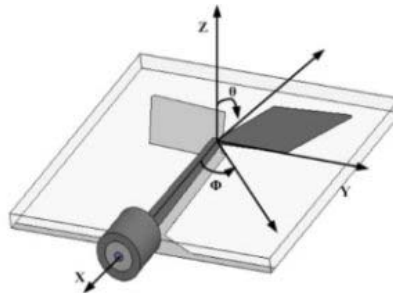**Figure 10.** Variation of input impedance with frequency.

Figure 11. Radiation pattern setup of proposed antenna.

an overall input impedance approximately $50\,\Omega$, i.e., characteristic impedance of coaxial cable over the entire band of operation.

Radiation pattern measurement setup is shown in Fig. 11. The antenna is placed in x-y plane with feeding probe from negative x axis. The angle 'θ' is drawn from z axis in clockwise direction and angle 'Φ' drawn from x axis in anticlockwise direction. Radiation patterns are simulated in two planes, E plane (X-Z) and H plane (Y-Z). $\Phi = 0°$ is E plane, and $\Phi = 90°$ is H plane.

Radiation patterns at all resonant frequencies $4.2\,\text{GHz}$, $6.6\,\text{GHz}$, $9.2\,\text{GHz}$, $12\,\text{GHz}$ and $15.8\,\text{GHz}$

are shown in Fig. 12. The measurement of radiation patterns is performed in an anechoic chamber by using two-port Agilent N5230A VNA. In radiation pattern measurement setup, the antenna under test (AUT) is placed on a rotator, and a double-ridged wideband horn antenna (2–18 GHz) is fixed at 1 meter distance apart from AUT. Then by fixing the specific orientation of horn antenna, AUT is rotated in E plane (X-Z) and H plane (Y-Z) by $360°$ with each step at $5°$. The measured and simulated radiation patterns of the proposed antenna for 4.2 GHz are nearly doughnut shaped in H plane and directional in E plane. But 6.6 GHz, 9.2 GHz, 12 GHz and 15.8 GHz radiation patterns in both planes are omnidirectional, which makes it a good candidate for wireless communication. The radiation patterns at 12.6 GHz and 16.2 GHz have some glitches. The glitches in radiation patterns can be attributed to the excitation of higher order modes at higher frequencies.

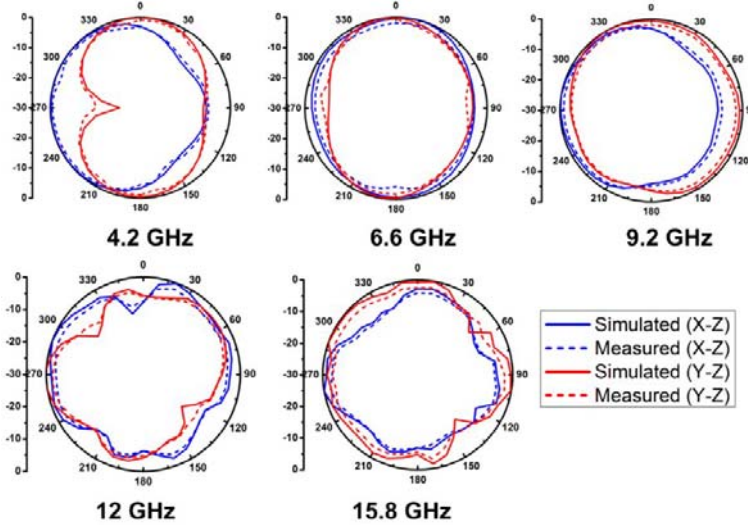Surface current density plots at resonance frequencies are shown in Fig. 13. It is observed that

Figure 12. Radiation patterns in both E plane (x-z) and H plane (y-z) of proposed antenna.

(a) 4.2 GHz   (b) 6.6 GHz   (c) 9.2 GHz
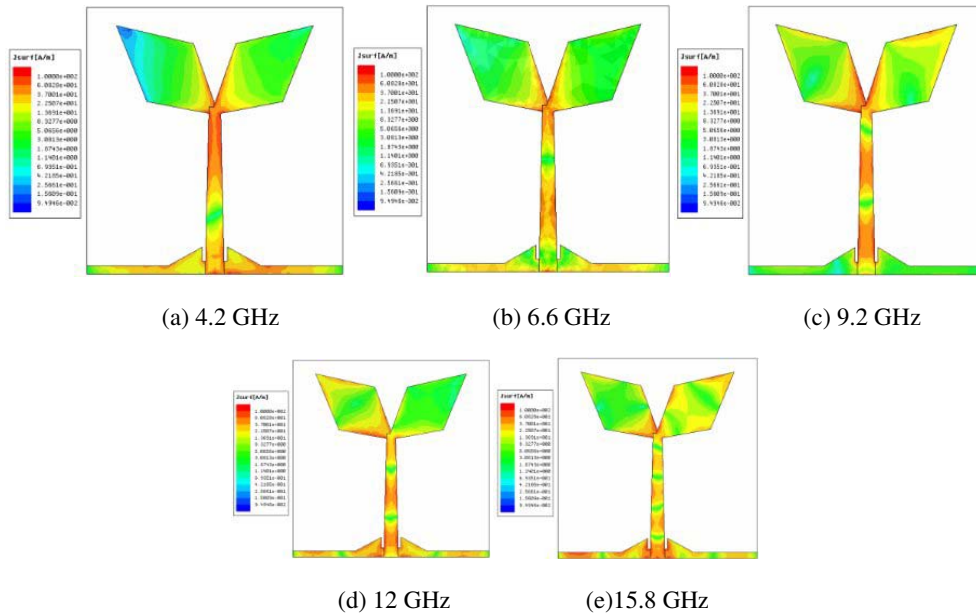
(d) 12 GHz   (e) 15.8 GHz

Figure 13. Surface current density of antenna at resonance frequencies.

surface current density at 4.2 GHz is concentrated on feeding edge of dipole elements shown in Fig. 13(a). At higher resonance frequencies current is distributed on the surface of patch as shown in Figs. 13(b)–13(e) and also on ground balun near feed region. So loading of slits on balun plays a significant role in impedance matching at these frequencies.

The variation of peak realised gain versus frequency is shown in Fig. 14. It is observed that the simulated peak gain varies between a maximum of 6.5 dB and minimum of 2.5 dB with an average of 3.6 dB. The measurement of gain is done in broadside direction ($\theta = 0°$ and $\Phi = 0°$) by using a setup as described for radiation pattern measurement, and the gain is calculated though the use of Friss's transmission equation. It is observed that the measured gain closely matches with simulated one. The gain increases with frequency along with some sharp dips which are due to poor impedance matching at some frequencies. Moreover, the gain changing depends on not only the frequency of operation, but also capture area which is a function of magnitude and phase of near-field distribution. There are changes in surface current distributions as shown in Fig. 13, that intensity of surface current in any active region of antenna changes with frequency significantly. So, there are some sharp changes in gain characteristics.
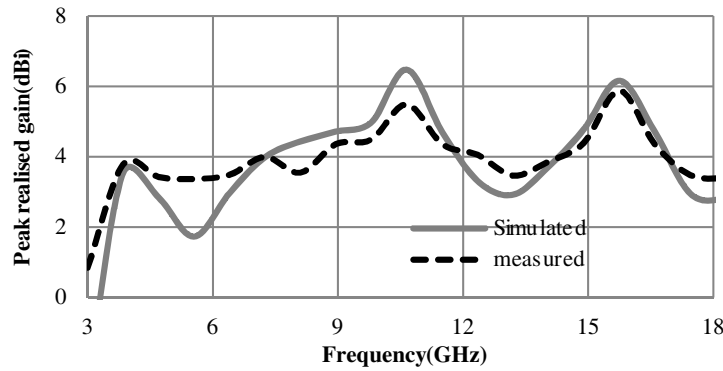
Figure 14. Peak realised gain of antenna versus frequency.

The simulated radiation and total efficiencies of the proposed antenna structure are given in Fig. 15. It is observed that the radiation efficiency is more than 70% and total efficiency more than 65% in obtained bandwidth. Efficiencies decrease with the increase in frequency and then stabilise at higher frequencies.
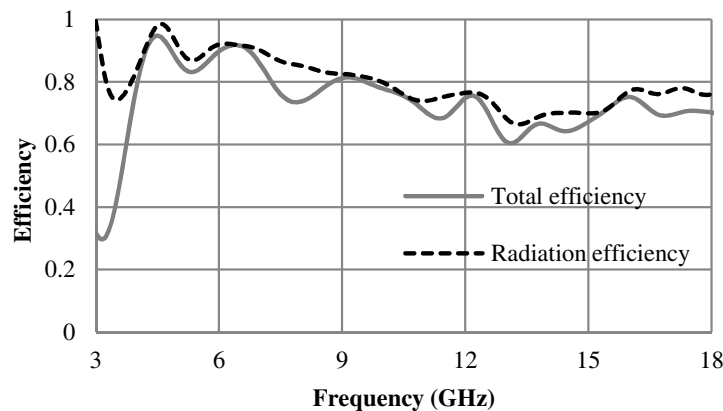
Figure 15. Efficiency versus frequency plot.

4. TIME DOMAIN STUDY

In designing UWB antennas, another crucial aspect to be analysed is its time domain performance and transfer function response. Therefore, important parameters, such as transmission coefficient (dB), phase of transmission coefficient and group delay, are studied by using CST MWS. For time domain analysis, two identical antenna structures are kept at a distance of 30 centimetres from each other in two configurations, i.e., face to face and side by side as shown in Fig. 16. A Gaussian impulse is transmitted through one antenna and received through a second antenna structure. Normalised amplitude of transmitted and received pulses in both configurations is shown in Fig. 17. There should be similarity between transmitted and received pulses. The correlation between transmitted and received pulses is calculated in terms of fidelity factor. If transmitted and received pulses match exactly then fidelity factor is 100%.
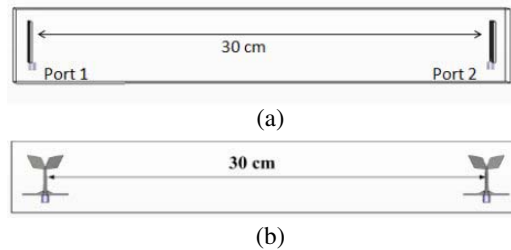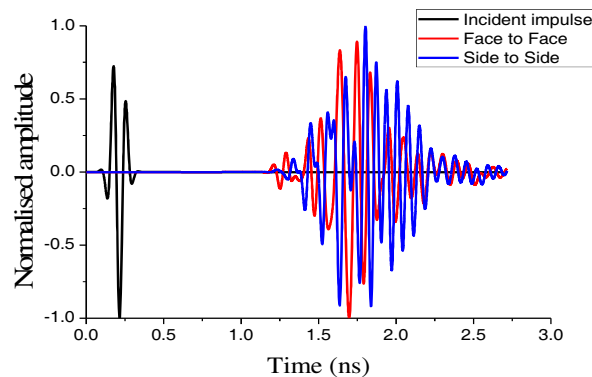

Figure 16. (a) Face to face. (b) Side by side.

Figure 17. Time domain normalised signal level.

The correlation coefficient or the fidelity factor is given by

$$
F = \max \left[\frac{\displaystyle\int_{-\infty}^{\infty} s_t(t)\, s_r(t - \tau)\, dt}{\displaystyle\int_{-\infty}^{\infty} |s_t(t)|^2\, dt \int_{-\infty}^{\infty} |s_r(t)|^2\, dt} \right]
$$

whereas $s_t(t)$ and $s_r(t)$ are the transmitted pulse and received pulse, and τ is the delay between transmitted and received pulses. The fidelity factor in both configurations, face to face and side by side, is shown in Table 4.

It can be seen from Fig. 18 that group delay is less than 2 ns in both configurations. At lower frequencies, the group delay varies from 0.4 to 1.8 ns for both the configurations, but as the frequency

Table 4. Fidelity factor for face to face and side by side configuration.

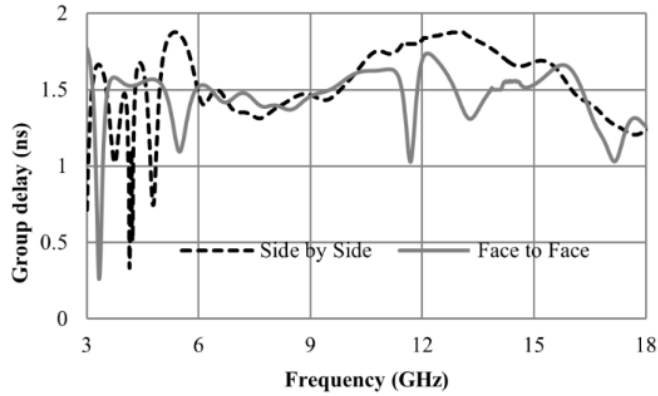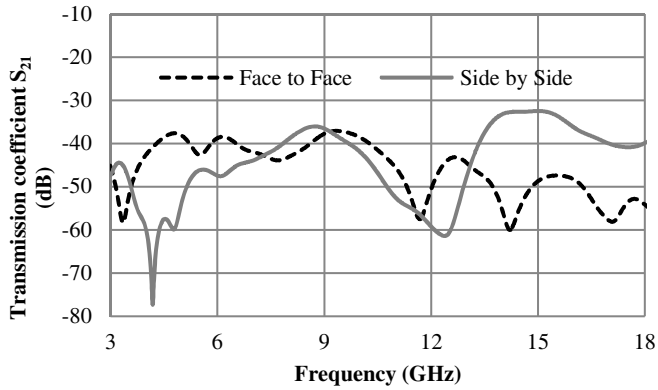| Configuration	Face to Face	Side by side
Fidelity Factor	0.82	0.78

Figure 18. Group delay characteristics.

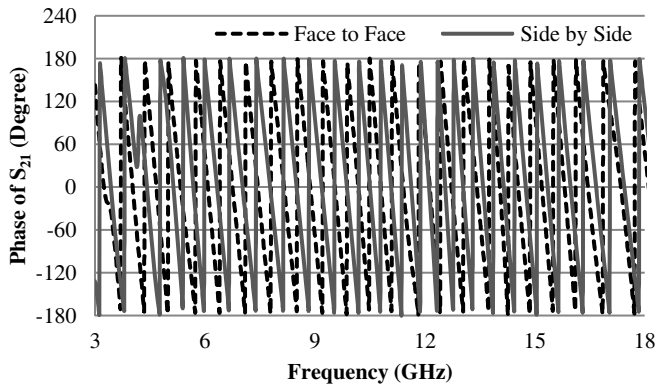**Figure 19.** Transmission coefficients S_{21} (dB) versus frequency.

Figure 20. Transmission coefficients S_{21} (phase) versus frequency.

is increased above 6 GHz, it is observed that the group delay has less variations, and peak value is up to 1.9 ns.

Variation of simulated transmission coefficient S_{21} (magnitude) for both configurations with frequency is shown in Fig. 19, which shows that transmission coefficient is below 30 dB throughout UWB band. At lower frequencies, side by side configuration has lower transmission coefficient than face to face configuration, but at higher frequencies, face to face configuration improves transfer response. It is observed from Fig. 20 that the phase of transmission coefficient is almost linear, so this antenna has less undesirable distortions.

The comparison between the proposed structure and available structures in literature, in terms of bandwidth and size, is listed in Table 5. It is observed in Table 5 that the dimensions of the proposed rotated quadrilateral antenna are low along with large bandwidth compared to other dipole antenna structures.

Table 5. Comparison of proposed antenna with other available antenna.

S. No.	Antenna	Size (mm^2)	% reduction in size	Bandwidth	
				GHz	In (%)
1	[4]	36×35	24	3–11	114.29
2	[5]	42×27	15	5.7–17.8	102.98
3	[6]	85×50	77	2.7–12	126.53
4	[7]	40×42.2	43	3.3–10.4	103.64
5	[8]	46×48	56	2.9–11.76	120.87
6	[9]	106×85	89	1.1–11	163.64
7	[10]	46×48	56	2.95–11.75	119.73
8	[11]	30.9×42.2	26	3.3–10.4	103.65
9	Proposed	31×31	-	3.8–18.1	130.91

5. CONCLUSION

A rotated quadrilateral dipole antenna for UWB applications is presented. The effect of rotation of patch element and two feed line structures on impedance matching is investigated. Moreover, the work on improving the performance of the balun structure is also performed. An agreement between the simulated and experimental results has proven the suitability of designed antenna structure for UWB applications. The antenna covers C-, X- and Ku-bands of microwave frequency spectrum. The antenna is suitable for future application of these microwave frequency bands.

ACKNOWLEDGMENT

REFERENCES

1. Federal Communications Commission, "First report and order, revision of part 15 of the commission's rule regarding ultrawideband transmission systems," FCC02-48, Apr. 22, 2002.
2. Lule, E., T. Babi, and K. Siwiak, "Analysis using FDTD of ultrawideband dipole antennas," *Antenna and Propagation Society International Symposium*, 2003.
3. Lule, E., T. Babi, and K. Siwiak, "Diamond dipole antenna for ultrawideband communication," *Microwave and Optical Technology Letters*, Vol. 46, 536–538, 2005.

4. Karacokak, T. and E. Topsakal, "A double sided rounded bow tie antenna for UWB communication," *IEEE Antennas and Wireless Propagation Letters*, Vol. 5, 446–449, 2006.

5. Eldek, A. A., "Ultrawideband double rhombus antenna with stable radiation patterns for phased array applications," *IEEE Transections on Antenna and Propagation*, Vol. 55, 84–91, 2007.

6. Liu, J., D. Zhao, and B. Z. Wang, "A beveled and slot loaded planer bow tie antenna for UWB application," *Progress In Electromagnetics Research M*, Vol. 2, 37–46, 2008.

7. Rave, C., T. Jaachke, B. Rohrdantz, and A. F. Jacob, "A curved edge dipole antenna for UWB applications," *Proceedings of 43rd European Microwave Conference*, 2013.

8. Gao, G. P., X. Xia, and Y. Jin, "Double printed rectangular patch dipole antenna for UWB applications," *Microwave and Optical Technology Letters*, Vol. 50, 2450–2452, 2008.

9. Zhang, J. P., Y. S. Xu, and W. D. Wang, "Ultra wideband microstrip fed planer elliptical dipole antenna," *Electronic Letter*, Vol. 42, 144–145, 2006.

10. Hu, Y. S., M. Li, G. P. Gao, J. S. Zhang, and M. K. Yang, "A double printed trapezoidal patch dipole antenna for UWB applications with band notched characteristics," *Progress In Electromagnetics Research*, Vol. 103, 259–269, 2010.

11. Lin, S., R. N. Cai, G. L. Huang, X. Y. Zhang, X. Q. Zhang, and L. Z. Wang, "Study of miniature UWB wafer dipole printed antenna fed by balanced microstrip line," *Progress In Electromagnetics Research C*, Vol. 19, 73–83, 2011.

12. Lizzi, L., F. Viani, R. Azaro, and A. Massa, "A PSO driven spline based shaping approach for ultrawide band antenna synthesis," *IEEE Transactions on Antennas and Propagation*, Vol. 56, 2613–2621, 2008.

13. Schantz, H., "Apparatus for establishing signal coupling between a signal line and an antenna structure," US patent 6,512,488, 2003.

14. Schantz, H. G., "Bottom fed planar elliptical UWB antennas (IEEE UWBST 2003)," *Proceedings of the IEEE UWBST Conference*, 2003.

15. "High frequency structure simulator (HFSS)," Ansoft[online] available : http://www.ansys.com.

16. CST Microwave Studio Suite 2011, CST Inc., 2007.